Supporting Information: Quantum interference assisted spin filtering in graphene nanoflakes

Angelo Valli,* Adriano Amaricci, Valentina Brosco, and Massimo Capone

Scuola Internazionale Superiore di Studi Avanzati (SISSA) and Democritos National Simulation Center, Consiglio Nazionale delle Ricerche, Istituto Officina dei Materiali (CNR-IOM), Via Bonomea 265, 34136 Trieste, Italy

E-mail: avalli@sissa.it

Phone: +39 040 3787 505

Emergence of magnetism: gap engineering and quantum fluctuations

In this section we discuss the values of the model parameters used for the calculations reported in the manuscript and their impact on our results. In particular we focus on the conditions for the onset of magnetism in our nanoflakes.

The estimate of realistic interaction parameters for Hubbard-like modeling of solids is still a highly debated and very controversial issue in solid-state physics. The value of the bare Hubbard interaction among π-electrons was computed by Parr et al.[1] as $U = 16.93$ eV. Assuming a value of $t \approx 2.8$ eV for graphene,[2] it yields an estimate $U/t \approx 6$. In order to obtain the effective U for a Hubbard model, one has to consider the effect of screening. In a relatively small nanostructure we can expect a poorer screening with respect to a graphene sheet because of the finite-size gap due to the confined geometry. Therefore we assume a value of $U/t = 3.75$.

We stress however that the message of the present manuscript does not rely on precise estimates of parameters. The basic requirement to exploit quantum interference as a spin filter is that magnetism sets in for the values of the interaction we consider. The relevance of magnetism in graphene nanostructures with ZZ edges has been indeed predicted in a variety of papers and, most importantly, has been found experimentally in small nanoribbons, where the magnetic ordering survives up to room temperature, strongly supporting the relevance of our results.

In a system with a finite spectral gap Δ the transition from the paramagnetic (PM) to the antiferromagnetic (AF) state inevitably sets in at a finite value of the Coulomb interaction (U_{AF}) which is mainly controlled by the amplitude of the gap. In particular, in graphene nanoflakes the quantum confinement gap Δ decreases as the inverse of the linear size of the nanoflake L, as explicitly shown in the numerical calculations reported in Fig. 1(c) of the manuscript, in agreement with theoretical and experimental results in the literature.[3,4] As a result, also the value of U_{AF} is suppressed upon increasing the size of the nanoflake. This is shown by our DMFT results in Fig. S1, where we show the average magnetization $\langle S^z \rangle$

of the nanoflake as a function of U/t, for nanoflakes of increasing size. Note that the value of U_{AF} decreases from $U_{AF}/t \approx 3.1$ to $U_{AF}/t \approx 2.0$, upon increasing the linear size of the nanoflake from $L \approx 14$ Å ($3N$ nanoflake) to $L \approx 25$ Å ($5N$ nanoflake).

It is important to stress, when comparing our results with previous literature, that our dynamical mean-field theory (DMFT) include quantum effects which tend to reduce the mean-field order parameter. This leads to a substantial increases of U_{AF} with respect to static mean-field approaches, which completely neglect quantum fluctuation leading to small values of U_{AF} for graphene nanoflakes.[5,6]

To be concrete, we refer to calculations for a $3N$ hexagonal nanoflake,[7] where it is estimated $U_{AF}/t \approx 2.0$ for static mean-field, and $U_{AF}/t \approx 3.1$ for DMFT. Therefore, for a $5N$ hexagonal nanoflake, the static mean-field value of $U_{AF}/t \approx 1.4$ indicated by Fernandez-Rossier and Palacio[5] is perfectly compatible with our $U_{AF}/t \approx 2.0$ DMFT estimate from Fig. S1.

Independently on the specific value of U/t chosen or the approximation employed, here we show that it is reasonably possible to realize magnetic nanoflakes also exploiting size engineering, i.e., lowering the value of U_{AF} by reducing the quantum confinement gap.

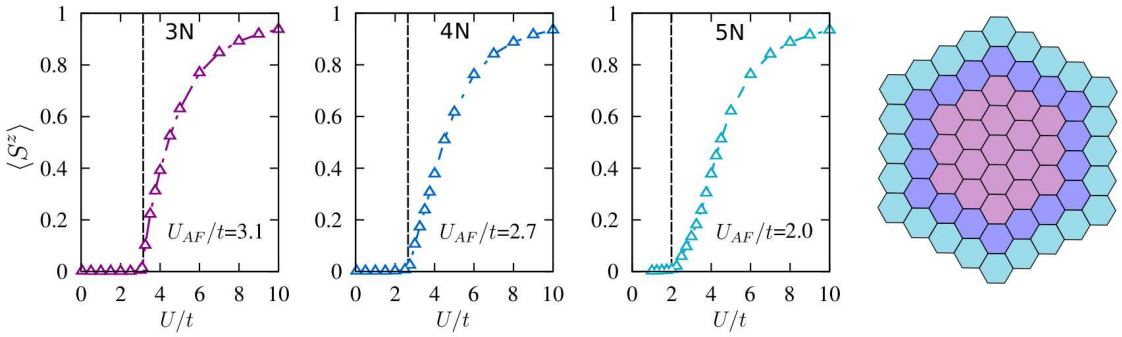

Figure S1: Average magnetization $\langle S^z \rangle$ as a function of U/t and corresponding numerical estimate of U_{AF}/t (dahsed line) for nanoflakes with $N = 3$, $N = 4$, and $N = 5$ edge atoms (right panel).

Effect of the hybridization to the leads

Transport properties in the weak- and strong-hybridization regime

In the following we show the effect of the hybridization between the $3N$ nanoflake and the leads on the QI antinode in the meta configuration. In particular, we show the evolution of $T(\omega)$ from the weak- to the strong-hybridization regime.

The interacting Green's function of the isolated nanoflake (indicated with an empty circle, $G_\circ$) is defined as

$$G_\circ(\omega) = \big(\omega + \mu - \Sigma(\omega)\big)^{-1}, \tag{1}$$

where μ is the equilibrium chemical potential of the nanoflake and $\Sigma(\omega)$ is the dynamical self-energy matrix that takes into account electron-electron correlations. In the presence of the leads, the Green's function of the device (indicated with a filled circle, $G_\bullet$) is calculated by solving the Dyson following equation

$$G_\bullet^{-1}(\omega) = G_\circ^{-1}(\omega) - \Sigma_L(\omega) - \Sigma_R(\omega), \tag{2}$$

where the leads are described by the embedding self-energy, defined as $\Gamma_\alpha(\omega) = -\frac{i}{2}\big(\Sigma_\alpha^r(\omega) - \Sigma_\alpha^a(\omega)\big)$, with $\alpha = L, R$ corresponding to the left (L) and right (R) leads.

In Fig. S2(a) we show the transmission coefficient $T(\omega)$ in the meta configuration (i.e., the one which exihibits a QI antinode) in the PM state. We show the evolution of $T(\omega)$ from the weak- ($\Gamma/t \approx 0.02$) to the strong-hybridization ($\Gamma/t \approx 0.25$) regimes. Upon increasing the hybridization we observe two main effects: i) the spectral features of the transmission become visibly broadened, and ii) the overall transmission increases (as the conductance $g \propto \Gamma^2$). However, due to destructive QI, the transmission at $\omega = 0$ is strongly suppressed at any value of Γ/t, demonstrating the robustness of the QI features in all hybridization regimes.

For the hexagonal nanoflake considered here $G_\circ(\omega)$ is invariant under the C_3 spatial

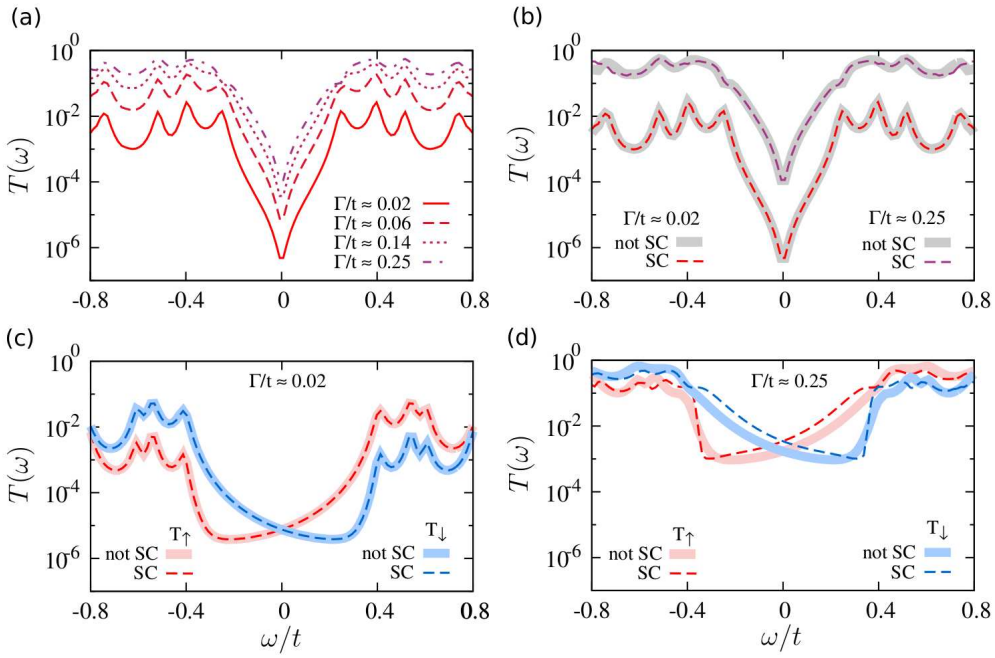

Figure S2: $T(\omega)$ in the meta configuration for the $3N$ nanoflake. **(a)** In the PM state: the QI antinode is robust by increasing the hybridization strength to the leads Γ/t. **(b)** Comparison between non-self-consistent (shaded area) and fully self-consistent (dashed line) treatment of the leads on the transmission in the weak- ($\Gamma/t=0.02$) and strong-hybridization ($\Gamma/t=0.25$) regimes. **(c-d)** Spin-resolved QI antinode in the AF state at $\Gamma/t = 0.02$ and $\Gamma/t = 0.25$, showing that the QI spin-filtering effect is robust against the values of Γ/t.

rotation symmetry on the graphene plane. However, the presence of the leads breaks the C_3 rotational invariance and lowers the symmetry of the system (in all contact configurations). Hence, in order to evaluate the transmission, it is necessary to calculate $G_\bullet$ and all observables fully self-consistently. For the sake of completeness, in Fig. S2(b) we also compare the meta transmission function $T(\omega)$ obtained in the weak- and strong-hybridization regimes, when the leads are taken into account self-consistently or when the Green's function of the isolated nanoflake is used to evaluate the transmission, showing that there is barely any difference in the resulting tranmission.

In Figs. S2(c,d) we show the same analysis in the AF state. Here, the leads perturb the distribution of the magnetic moments with respect to the isolated nanoflake, and the local magnetic moment $\langle S_i^z \rangle$ in the proximity of the corresponding edges are partially quenced (up to 30% in the strong-hybridization limit). However, the splitting between the spin-resolved

QI antinodes $\Delta\omega = \omega_{\uparrow}^{QI} - \omega_{\downarrow}^{QI}$ does not depend on the magnetic pattern within the nanoflake, but is controlled by the average staggered magnetization $\langle S^z \rangle$, which is, instead, only weakly affected by the leads. As a consequence, minor differences can be observed in the strong-hybridization limit (e.g., the position of ω_{σ}^{QI} change slighly) but the QI-assisted spin-filtering effect remains robust. Remarkably, while this effect is reasonable for large nanoflakes with lower surface-to-bulk ratio, we find this to be true even for the $3N$ nanoflake, which has a linear size of $L \approx 14$ Å, and a surface-to-bulk ratio of 1/3. As a result, the spin-resolved QI antinode in the AF state is a robust feature of graphene nanoflake junctions, almost independently on size.

Transport properties beyond the wideband limit (WBL)

In the wide-nad limit (WBL), the embedding self-energy of the leads is a purely imaginary constant $\Sigma_{L/R}(\omega) = -\imath\Gamma$, which it contributes to the broadening of the many-body states of the nanoflake. A realistic hybridization to the leads would also include a real part which instead shifts the poles of the Green's function.

The applicability of the WBL in transport calculations has been discussed in details by Verzijl et al.,[8] concluding that WBL qualitatively reproduces the main features of the transmission and the bias-voltage dependence in cases where the transmission is dominated by the properties of the molecule. This sheds a positive light on our work, as the fundamental feature for the realization of the spin-filtering effect is indeed a property of the molecule, i.e., the destructive QI, and not the hybridization with the contacts.

Nevertheless, in order to understand the possible effect of a realistic hybridization function on the transport properties, in the following we consider and explicitly take into account the effects of the leads beyond the WBL, and we present transport calculations with a semi-circular (Bethe) density of states with a finite bandwidth D for the leads. The corresponding

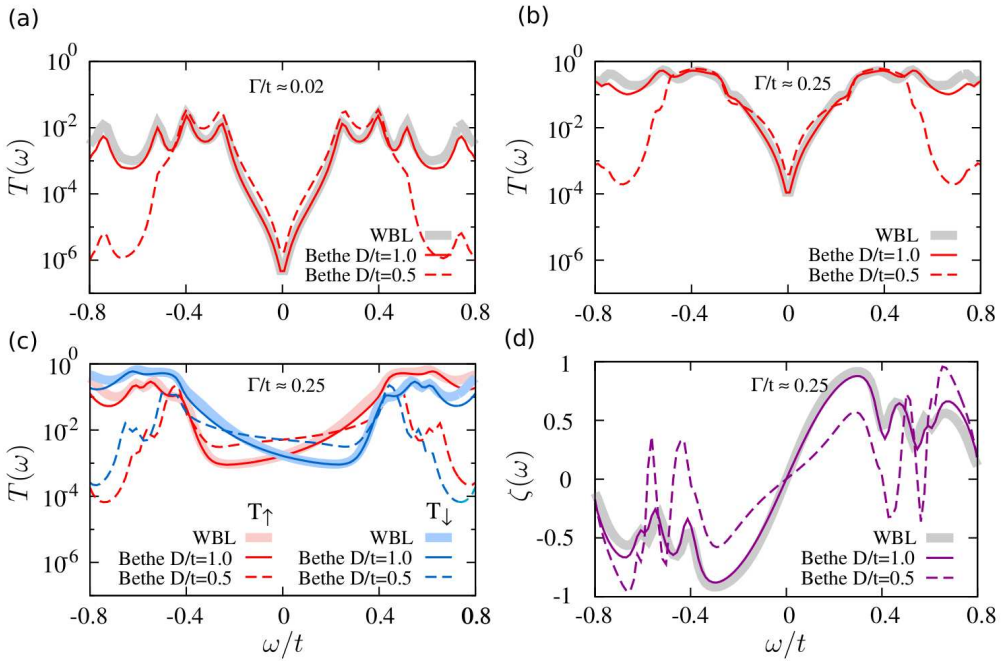

Figure S3: $T(\omega)$ in the meta configuration for the $3N$ nanoflake comparing the wide-band limit (WBL) and a Bethe density of states for the leads. **(a,b)** In the PM state: the QI antinode is robust by increasing the hybridization strength to the leads Γ/t. **(c)** In the AF state: the QI antinote is robust. Some quantitative deviations can be observed with respect to the WBL in the extreme case in which the hybridization is strong ($\Gamma/t = 0.25$) and the edge of the leads' DOS lies at the edge of the AF gap (i.e, for $D/t = 0.5$). **(d)** Spin-polarization of the transmission: even in the most unfavorable case the polarization is suppressed up to about 30%, but the spin-filtering effect survives.

embedding self-energy reads

$$\Sigma(\omega) = V^2 \frac{4}{\pi} \sum_k \frac{1}{\omega + \mu - \epsilon_k} \sqrt{1 - \left(\frac{\epsilon_k}{D}\right)^2}. \tag{3}$$

In order to compare the Bethe lead with the WBL, we chose the hybridization parameter V so that $\Gamma \equiv -V^2 \int_{-\infty}^{\infty} d\omega \Im\Sigma(\omega)/\pi$ for the Bethe leads is equal to the value of Γ in the WBL. The results are shown in Figs. S3(a,b) for the PM state, and Figs. S3(c,d) for AF state. At low-energy, the calculations with the Bethe DOS reproduces the $T(\omega)$ of the WBL both in the weak- and in the strong-hybridization regimes (Figs. S3(a) and S3(b), respectively). Obviously, the transmission is suppressed for $|\omega| > D$, but in the limit $D \gg t$, also the high-energy features would be recovered. The situation is more complex in the AF state,

because the QI antinote is found at a finite frequency $|\omega_\sigma^{QI}| \propto \langle S^z \rangle$. In particular, if the edge of the Bethe DOS, where $\Re\Sigma_{L/R}(\omega)$ is the largest, is located in proximity of ω_σ^{QI}, one can observe some deviations from the WBL, as in Fig. S3(c) for $D/t = 0.5$. However, even in this case, which is the most unfavorable for the realization of the QI assisted spin-filtering effect, the spin polarization $\zeta(\omega) = (T_\uparrow - T_\downarrow)/(T_\uparrow + T_\downarrow)$ is found to be suppressed at most about 30%. This makes the efficiency of the device suboptimal but it does not destroy its spin-filtering properties.

We can conclude that the details of the DOS of the leads is generally irrelavant to the realization of the QI assisted spin-filtering effect. Together with the symmetry analysis that we discussed in the manuscript, these numerical calculations confirm that the phenomenon is a robust features of graphene junctions, and sheds promising lights on its experimental realization.

Effects of symmetry breaking on the destructive QI

In the manuscript we show that the QI features of graphene nanostructures can be understood in terms of the symmetries of the Hamiltonian, which establish their robustness and generality. However, the existence of QI features does *not* rely on those symmetries, and that indeed the QI antiresonances appear in the transmission even when the symmetries are lifted. Here we show that the QI properties survive even if those symmetries are broken. We focus on two case: i) when the particle-hole symmetry is broken by the presence of hoppings beyond nearest neighbors (NN), and ii) when the chiral symmetry of graphene is broken by the presence of a substrate.

Structural electron-hole asymmetry: $t' \neq 0$

As a matter of fact, in actual graphene nanostructures the particle-hole symmetry of NN hopping tight-binding Hamiltonian, as considered above, is expected to be broken by hopping

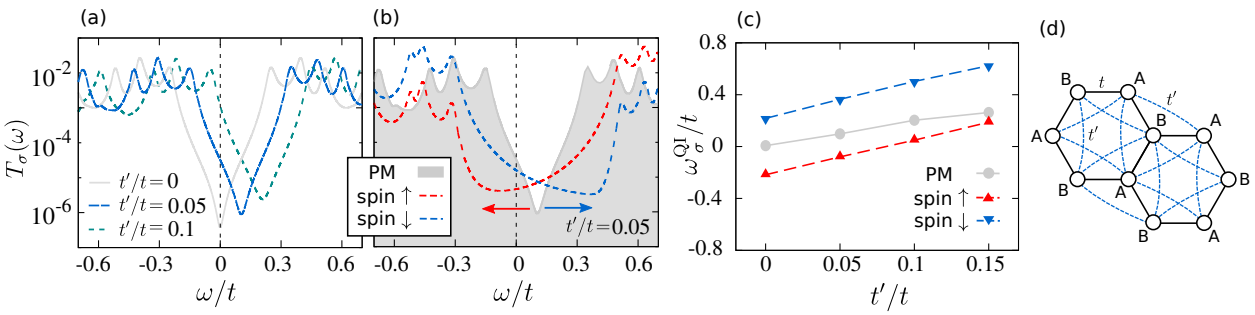

Figure S4: **(a-b)** Transmisson coefficient in the PM and AF state for different values of the particle-hole symmetry breaking t'/t for $\Gamma/t = 0.02$ and $U/t = 3.75$. **(c)** Shift of the QI antinode ω^{QI} as a function t'/t. **(d)** While NN hopping t connect atoms from different sublattices (AB), the next-NN hopping t' connects atoms within the same sublattice (AA or BB).

processes beyond NN or by lattice deformations. Here we consider the case in which we include next-NN hopping $t' \neq 0$ in the tight-binding Hamiltonian.

In Fig. S4(a) we show explicitly that t' does not destroy the QI antiresonance, but it shifts the frequency $\omega^{\rm QI}$ (at which the destructive interference takes place) at finite energy. We can understand this result observing that t' shifts the DOS, so that the chemical potential no longer lies in the middle of the gap, but slightly below (for positive t'/t). However, if the spectrum at $t'=0$ was symmetric around $\omega=0$, it still possesses a *near symmetry* around a shifted energy $\omega^{QI} \neq 0$. In particular, here $\omega^{QI} \propto t'/t$. This, in turn, results in a zero of the Green's function at the same energy, away from the Fermi level.

It is also important to notice that a relatively small next-NN hopping, besides driving the system away from half-filling, does not destroy the ordered AF state due to the presence of the quantum confinement gap. In the AF state we observe that $T_\uparrow(\omega)$ and $T_\downarrow(\omega)$ are split around the antiresonance energy ω^{QI}, as shown in Fig. S4(b) for $t'/t=0.05$.

While a finite t' is a simple conceptual handle to tune the position of the QI antiresonance, this parameter is not easily tuned in actual materials. Similar effects can be obtained using deformations of the lattice structure induced by applying, e.g., strain. The possibility to mechanically control QI has been recently demonstrated experimentally for π-stacked dimers exhibiting destructive QI.[9] Yet, in complex nanostructures it may be difficult to achieve a

precise control over the local lattice deformations and ultimately on the position of the QI antiresonance.

Chiral symmetry breaking: graphene/h-BN(0001)

Upon deposition of graphene on hexagonal boron-nitride (h-BN) the two inequivalent A and B sublattices experience a different chemical environment due to asymmetric absorption on the substrate. This effect can be modeled by the following substrate Hamiltonian[10]

$$H_{\rm sub} = -\sum_i \left(\epsilon_A n_{iA} + \epsilon_B n_{iB}\right), \tag{4}$$

where $n_{iA(B)}$ is the electron density operators at site i on sublattice $A(B)$ and $\epsilon_A = -\epsilon_B = \epsilon$ is the parameter that measures the degree of chiral symmetry-breaking.

The term in Eq. (4) induces a charge modulation between the two sublattices, as the occupation of all sites deviates from half-filling. This is quantified by the charge-density wave order parameter $\Delta_{\rm CDW} = N_C^{-1}\sum_i \left(n_{iA} - n_{iB}\right)$, with N_C the number of C atoms in the nanostructure. As a consequence, also the local magnetic moments $\langle S_i^z\rangle$ are partially quenced, and the staggered magnetization $\langle S^z\rangle = N_C^{-1}\sum_i \left(\langle S_{iA}^z\rangle - \langle S_{iB}^z\rangle\right)$ is reduced. However, the AF pattern of the magnetization is nevertheless preserved.

In Fig. S5 we show the amplitude of $\Delta_{\rm CDW}$ and $\langle S^z\rangle$ for the isolated $3N$ nanoflake at $U/t = 3.75$, as a function of the hybridization between the nanoflake and the substrate.

In order to compare the effects of the chiral symmetry-breaking field ϵ in all contact configurations, in Fig. S6 we show the ortho, meta, and para transmission coefficient $T_\sigma(\omega)$ of the $3N$ nanoflake device. In general, for the ortho and para configurations (which do not display destructive QI) the polarization in the proximity of the Fermi level is lower than in the meta configuration. For each spin polarization σ, the transmission coefficient in the ortho and para configurations fulfills the condition $T_\sigma(\omega) = T_\sigma(-\omega)$ (while the substrate breaks the relation between spin $\uparrow$ and $\downarrow$). As a result, there is a finite $\Delta T(0) = T_\uparrow(0) - T_\downarrow(0)$ but

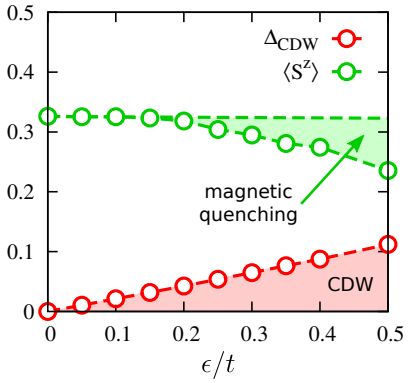

Figure S5: Amplitde of the charge-density wave Δ_{CDW} order parameter and the staggered magnetization $\langle S^z \rangle$ for the isolated $3N$ nanoflake at $U/t = 3.75$.

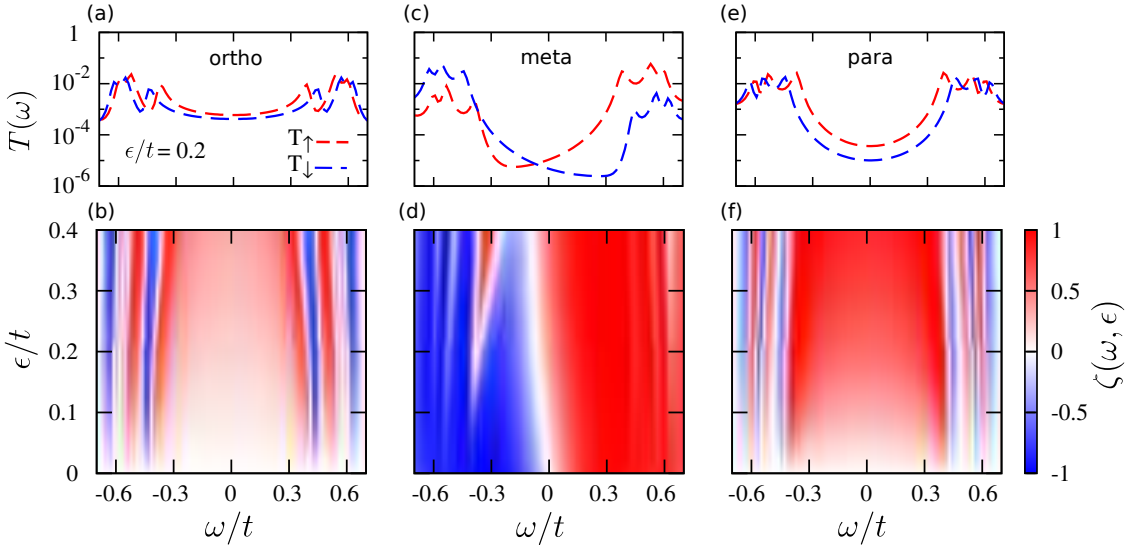

Figure S6: Transmission coefficient for $\epsilon/t = 0.2$ and heatmap of the spin-polarization $\zeta(\omega, \epsilon)$ in the ortho **(a-b)**, meta **(c-d)**, and para **(e-f)** configurations for the $3N$ nanoflake, for $\Gamma/t = 0.02$ and $U/t = 3.75$.

the local minimum of the transmission is pinned at the Fermi level. Eventually, this is the reason why the corresponding spin-current J_s is lower than in meta configuration.

Therefore, we can conclude that the suppression of the transmission in one spin channel, due to spin-resolved destructive QI achieved in the meta configuration, is fundamental in order to obtain an efficient spin filter. In particular, QI-assisted spin-filtering is more effective than any polarization induced in the ortho or para configurations.

References

(1) Parr, R. G.; Craig, D. P.; Ross, I. G. *J. Chem Phys.* **1950**, *18*, 1561.

(2) Neto, A. H. C.; Guinea, F.; Peres, N. M. R.; Novoselov, K. S.; Geim, A. K. *Rev. Mod. Phys.* **2009**, *81*, 109.

(3) Ritter, K. A.; Lyding, J. W. *Nat. Mat.* **2009**, *8*, 235–242.

(4) Hu, W.; Lin, L.; Yang, C.; Yang, J. *J. Chem. Phys.* **2014**, *141*, 214704.

(5) Fernández-Rossier, J.; Palacios, J. J. *Phys. Rev. Lett.* **2007**, *99*, 177204.

(6) Gunlycke, D.; Areshkin, D. A.; Li, J.; Mintmire, J. W.; White, C. T. *Nano Lett.* **2007**, *7*, 3608–3611.

(7) Valli, A.; Amaricci, A.; Toschi, A.; Saha-Dasgupta, T.; Held, K.; Capone, M. *Phys. Rev. B* **2016**, *94*, 245146.

(8) Verzijl, C. J. O.; Seldenthuis, J. S.; Thijssen, J. M. *J. Chem. Phys.* **2013**, *138*, 094102.

(9) Frisenda, R.; Janssen, V. A. E. C.; Grozema, F. C.; der Zant, H. S.; Renaud, N. *Nat. Chem.* **2016**, *8*, 1099–1104.

(10) Skomski, R.; Dowben, P. A.; Driver, M. S.; Kelber, J. A. *Mater. Horiz.* **2014**, *1*, 563–571.